Volume 10 | Number 19 | 21 May 2014 | Pages 3349–3514

Soft Matter

www.softmatter.org

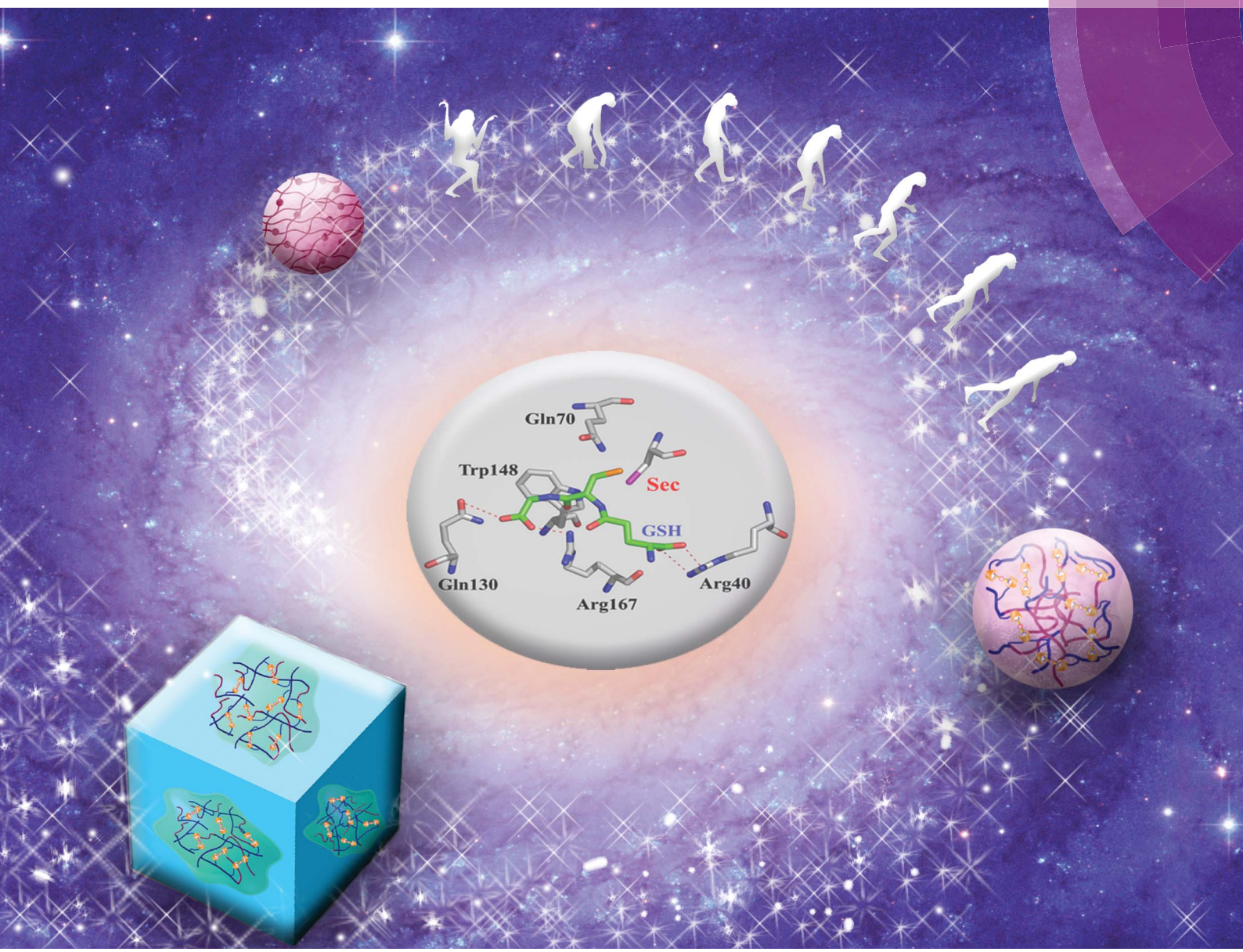

ISSN 1744-683X

ROYAL SOCIETY OF CHEMISTRY

PAPER

Yanzhen Yin, Shufei Jiao *et al.*

A supramolecular microgel glutathione peroxidase mimic with temperature responsive activity

Soft Matter

PAPER

View Article Online
View Journal | View Issue

A supramolecular microgel glutathione peroxidase mimic with temperature responsive activity

Cite this: *Soft Matter*, 2014, **10**, 3374

Yanzhen Yin,*[ab] Shufei Jiao,*[a] Chao Lang[c] and Junqiu Liu[c]

Glutathione peroxidase (GPx) protects cells from oxidative damage by scavenging surplus reactive oxygen species (ROS). Commonly, an appropriate amount of ROS acts as a signal molecule in the metabolism. A smart artificial GPx exhibits adjustable catalytic activity, which can potentially reduce the amount of ROS to an appropriate degree and maintain its important physiological functions in metabolism. To construct an optimum and excellent smart artificial GPx, a novel supramolecular microgel artificial GPx (**SM-Te**) was prepared based on the supramolecular host–guest interaction employing the tellurium-containing guest molecule (**ADA-Te-ADA**) and the cyclodextrin-containing host block copolymer (poly(*N*-isopropylacrylamide)-*b*-[polyacrylamides-*co*-poly(6-*o*-(triethylene glycol monoacrylate ether)-β-cyclodextrin)], **PPAM-CD**) as building blocks. Subsequently, based on these building blocks, **SM-Te** was constructed and the formation of its self-assembled structure was confirmed by dynamic light scattering, NMR, SEM, TEM, *etc.* Typically, benefitting from the temperature responsive properties of the PNIPAM scaffold, **SM-Te** also exhibited similar temperature responsive behaviour. Importantly, the GPx catalytic rates of **SM-Te** displayed a noticeable temperature responsive characteristic. Moreover, **SM-Te** exhibited the typical saturation kinetics behaviour of a real enzyme catalyst. It was proved that the changes of the hydrophobic microenvironment and the pore size in the supramolecular microgel network of **SM-Te** played significant roles in altering the temperature responsive catalytic behaviour. The successful construction of **SM-Te** not only overcomes the insurmountable disadvantages existing in previous covalent bond crosslinked microgel artificial GPx but also bodes well for the development of novel intelligent antioxidant drugs.

Received 15th December 2013
Accepted 9th February 2014

DOI: 10.1039/c3sm53117a

www.rsc.org/softmatter

Introduction

Reactive oxygen species (ROS) (hydrogen peroxides, organic hydroperoxides and phospholipid hydroperoxides) are the byproducts of cellular metabolism, which are normally harmless to humans and act as signal molecules in the metabolism.[1] However, surplus ROS can lead to many human oxidative stress-related diseases such as reperfusion injury, inflammatory process, neuronal apoptosis and cancer.[2,3] Generally, such oxidative stress-related diseases are controlled by the antioxidative defense system, especially by the antioxidative enzyme system. Especially, as a member of the family of antioxidative enzymes, glutathione peroxidase (GPx, Ec.1.11.1.9) is an important selenium-containing enzyme, which catalyzes the reduction of hydroperoxides (ROOHs) using glutathione (GSH) as the substrate.[4,5] Owing to its biologically crucial role, considerable efforts have been devoted to produce organoselenium/tellurium compounds that mimic the properties of GPx in recent years.[6–16] In our group, based on the understanding of the structure of a native GPx, some artificial GPxs have been designed employing the imprinting method,[13] ATRP[17,18] and blending process.[19,20]

A microgel is a cross-linked polymer particle, which has been first described by Staudinger.[21] Recently, polymer microgels have been proven to be excellent scaffolds for biomaterials.[22,23] Due to the unique property of combing the characteristics of a linear macromolecule and a three-dimensional network, polymer microgels have been widely used in the fields of artificial enzymes,[22,24] regenerative medicines,[25] sensors,[26] drug delivery systems,[27] and so on. Especially, the microgel is one of the most suitable scaffolds for an artificial enzyme as its three-dimensional space network is similar to the folding secondary structure of the native enzyme. Therefore, various artificial enzymes are constructed based on microgels.[22,24,28,29] In our previous report, we have successfully constructed a covalent bond crosslinked microgel artificial GPx based on a temperature-responsive microgel using poly(*N*-isopropylacrylamide) (PNIPAM) as the scaffold (this smart artificial GPx is denoted as **Microgel GPx** in this report).[24] Considering that **Microgel GPx**

[a]*School of Chemistry and Chemical Engineering, Qinzhou University, No. 89, Xihuan Nanlu, Qinzhou 535000, People's Republic of China. E-mail: yinyanzhen2013@163.com; jiaoshufei2013@163.com; Fax: +86-0777-2860226*

[b]*Guangxi Experiment Centre of Science and Technology, Guangxi University, Nanning 530004, China*

[c]*State Key Laboratory of Supramolecular Structure and Materials, Jilin University, Changchun 130012, People's Republic of China*

exhibited controllable catalytic activity, it could potentially be applied to exploring intelligent antioxidant drugs for adjusting the appropriate concentration of ROS as only surplus ROS could result in various illnesses. However, there were still two serious and insurmountable disadvantages in **Microgel GPx**. On the one hand, the synthetic process of the covalent bond crosslinked microgel was carried out employing cetyl trimethylammonium bromide (CTAB) as the surfactant. The efficient separation of CTAB from the microgel solution during the purification process was not achievable. On the other hand, the synthetic polymers with higher molecular weight can commonly elicit a strong immune response and are difficult to be degraded or excreted by the metabolic system when they were potentially used as scaffolds for smart antioxidant drugs.[30–32] Herein, **Microgel GPx** exhibited the average diameter of 160 nm and its molecular weight was far higher than that of the traditional single chain polymer. Thus, this microgel was difficult to be degraded or excreted by the metabolic system. These two disadvantages have largely limited the further application of **Microgel GPx**. Therefore, how to overcome these two insurmountable disadvantages, design a novel smart artificial GPx, and provide an optimum and excellent scaffold for the development of antioxidant drugs are still great challenges.

Since supramolecular chemistry has emerged as a fascinating field and is expanded into many interdisciplinary fields, versatile supramolecular materials have been designed.[33–38] Among these materials, supramolecular hydrogels are widely investigated. Due to the unique structure formed through non-covalent interactions, supramolecular hydrogels exhibit a reversible dynamic formation process,[39,40] and are extensively applied in the fields of sensors,[41,42] controlled release systems,[43,44] artificial enzymes[45,46] as well as self-healing materials.[47,48] These materials are also endowed with potential degradability due to the unique property of non-covalent interactions in supramolecular hydrogels. Amazingly, compared with supramolecular hydrogels, supramolecular microgels exhibited the additional advantages of low solution viscosity and nano-sized aggregation morphology, which provided an excellent scaffold for nano-sized biomaterials.[28,49,50] Commonly, the construction of supramolecular microgels can be easily achieved, which is like the '*stacker game*' using functional building blocks. Thus, desirable purity and productivity of the supramolecular microgel are obtained. Moreover, considering that the structure of the supramolecular microgel can be easily disassembled due to its dynamic and reversible self-assembled properties, the biomaterials based on supramolecular microgels can be easily degraded under appropriate conditions. Therefore, the supramolecular microgel with these unique properties can be employed to overcome the two insurmountable disadvantages existing in **Microgel GPx**. To construct the excellent smart artificial GPx with adjustable catalytic activity, effective preparation process and potential degradable ability, the combination of the artificial GPx and the supramolecular microgel is desirable.

Herein, the novel supramolecular microgel artificial GPx (**SM-Te**) was crosslinked by the host–guest interaction between cyclodextrin and adamantine. Such a host–guest interaction has been proved to be the efficient non-covalent interaction for the construction of supramolecular materials.[47,51–53] As a novel smart artificial GPx, **SM-Te** displayed a noticeable temperature responsive catalytic activity and the typical saturation kinetics behaviour of a real enzyme catalyst. To the best of our knowledge, **SM-Te** constructed in this work is the first example of a smart artificial GPx based on the scaffold of a supramolecular microgel. We anticipate that this artificial GPx not only bodes well for exploration of intelligent antioxidant drugs but also highlights the application of host–guest self-assembled supramolecular materials.

Experimental section

Materials

Tris(2-dimethylaminoethyl)amine (Me_6TREN) was synthesized as described previously.[54] *N*-Isopropylacrylamide (NIPAM, Aldrich) was recrystallized from hexane and toluene, and dried under vacuum prior to use. Sodium borohydride and 3-bromo-1-propanol were purchased from Fluka and were used without further purification. Cumene hydroperoxide (CUOOH), H_2O_2, and NBT were purchased from J&K Scientific Ltd and were used without further purification. 3-Carboxyl-4-nitrobenzenethiol (TNB) was synthesized from 5,5′-dithiobis(2-nitrobenzoic acid) as described previously.[12] Acrylamide, β-cyclodextrin, triethylamine, tetrahydrofuran, phenyl methanol and 4-toluene sulfonyl chloride were purchased from Shanghai Reagent Co. Acryloyl chloride and 2-bromopropionyl bromide were purchased from Anhui Wotu Reagent Co. Triethylamine and tetrahydrofuran were rigorously dried with sodium. 1-[*p*-(Phenyl-azo) phenoxyethyl]pyridinium bromide (**AZO**) was endowed from Liu's group.

Instrumentation

The characterization of the structures of the compounds was performed with a Bruker 300 MHz spectrometer using a TMS proton signal as the internal standard. UV-vis spectra were obtained using a Pgeneral T6 UV-vis spectrophotometer. Scanning electron microscopy (SEM) observations were carried out using a JEOL JSM-6700F scanning electron microscope with a primary electron energy of 3 kV. Transmission electron microscopy (TEM) observations were carried out using a JEOL JEM 3010 scanning electron microscope. The buffer pH values were determined with a METTLER TOLEDO 320 pH meter. Dynamic light scattering experiments were performed using a Malvern ZETAS12-ERNANOSERIES instrument. Molecular weights and molecular weight distributions were determined by GPC using THF as the eluent at a flow rate of 1.0 mL min^{-1}.

Characterization of ADA-Te-ADA, AZO and CD-monomer

ADA-Te-ADA was synthesized according to the preparation method of bis-(3-acryloyloxypropyl)-telluride in our previous report except that acryloyl chloride was replaced by 1-adamantanecarbonyl chloride.[24] **AZO** was endowed from Liu's group. The cyclodextrin containing a host monomer (6-*o*-(triethylene glycol monoacrylate ether)-β-cyclodextrin, **CD-monomer**) was synthesized according to our previous report.[19] The structures of them were determined using a Bruker 300 MHz spectrometer using a TMS proton signal as the internal standard.

ADA-Te-ADA. ^{1}H NMR (300 MHz, $CDCl_3$) δ (ppm) 4.09 (t, 2H), 2.66 (t, 2H), 2.07 (m, 2H), 2.01 (s, 3H), 1.88 (s, 6H), 1.71 (s, 6H).

AZO. ^{1}H NMR (300 MHz), $(CD_3)_2SO$ δ (ppm) 9.17 (d, 2H), 8.66 (t, 1H), 8.21 (t, 2H), 7.90–7.81 (m, 4H), 7.60–7.52 (m, 3H), 7.13 (d, 2H), 5.10 (t, 2H), 4.65 (t, 2H).

CD-monomer. ^{1}H NMR (300 MHz, D_2O) δ (ppm) 8.02 (s, 1H), 5.95–6.41 (m, 3H), 5.15 (s, 2), 5.00 (d, 7), 4.29 (t, 2H), 3.45–3.90 (m 56H (14H of glycol and 42H of cyclodextrin)).

Synthesis of PPAM-CD

The macroinitiator **PNIPAM-Br** and the cyclodextrin-containing host block copolymer (poly(*N*-isopropylacrylamide)-*b*-[polyacrylamides-*co*-poly(6-*o*-(triethylene glycol monoacrylate ether)-β-cyclodextrin)], **PPAM-CD**) were synthesized according to our previous report.[20] GPC analysis of **PNIPAM-Br** revealed a M_n of 8036 and a polydispersity, M_w/M_n, of 1.18. The M_n of **PPAM-CD** was 14 840. The polydispersity of **PPAM-CD** was 1.33. The concentration of cyclodextrin in **PPAM-CD** was estimated to be 3.2×10^{-4} mmol mg^{-1} according to the NMR analysis.

LCST determination of PPAM-CD

The determination of LCST was carried out according to the previously reported method.[64] Typically, the optical transmittance of the **PPAM-CD** solution (1 mg mL^{-1}) at different temperatures was measured at 600 nm using a Pgeneral T6 UV-vis spectrophotometer. Sample cells were thermostatted in a circulator bath at different temperatures from 25 to 45 °C prior to the measurements. The LCST was defined as the temperature of the 50% transmittance point during the first heating ramp. The LCST of **PPAM-CD** was 34.4 °C.

Preparation of supramolecular microgel SM-Te

Deionized water (9.5 mL) was introduced into a 25 mL flask. **PPAM-CD** (31.3 mg, 0.01 mmol) was added and dissolved in this solution. **ADA-Te-ADA** (2.85 mg, 0.005 mmol) was dissolved in methanol (0.5 mL). The solution of **PPAM-CD** was thermostatted in a circulator bath at 35 °C (above the LCST of **PPAM-CD**) for 10 min. Then, the methanol solution of **ADA-Te-ADA** was slowly added into the solution of **PPAM-CD** under sonication at 35 °C. After the dropwise process was finished, the mixture solution was treated under continual sonication at 35 °C for 20 min. Then, the supramolecular microgel **SM-Te** was obtained with a concentration of 3.42 mg mL^{-1}. The concentration of tellurium (catalytic center) was 0.5 mM.

LCST determination of SM-Te

The determination of optical transmittance of the **SM-Te** (1 mg mL^{-1}) solution at different temperatures was performed using a similar method to that of **PPAM-CD**. The LCST of **SM-Te** was 32.8 °C.

Determination of GPx activity

The catalytic activity was assayed according to a modified method reported by Hilvert *et al.*[6] Typically, the reaction was carried out at 25 °C in a 1 mL quartz cuvette, 700 μL of phosphate buffer (pH = 7.0. 50 mM) and 100 μL of the **SM-Te** (10 μM) were added, and then 100 μL of the TNB solution (1.5 mM) was added. The mixture in the quartz cuvette was pre-incubated at appropriate temperature for 3 min. Finally, the reaction was initiated by the addition of 100 μL of cumene hydroperoxide (CUOOH) (2.5 mM), and the absorption decrease of TNB at 410 nm (ε_{410} = 13 600 M^{-1} cm^{-1}, pH = 7.0) was monitored using a Pgeneral T6 UV-vis spectrophotometer. Appropriate control of the non-enzymatic reaction was performed and was subtracted from the catalyzed reaction.

Investigation of the stability of SM-Te

The stability of **SM-Te** was assayed based on the catalytic activity of **SM-Te** and the recycled **SM-Te**. Their catalytic activity was determined using the same method mentioned above (section of Determination of GPx activity). Typically, the recycling process of **SM-Te** and determination of catalytic activity were as follows: first, the catalytic reaction for the reduction of cumene hydroperoxide (CUOOH) by 3-carboxyl-4-nitrobenzenethiol (TNB) was carried out in a 1 mL quartz cuvette using the traditional method (see Determination of GPx activity). Secondly, the solution of **SM-Te** and other compounds of the assay system in a 1 mL quartz cuvette was recycled. The solvent of this solution was removed using a rotary evaporator and the recycled compound (**SM-Te** and other compounds of the assay system) was dried under vacuum for 24 h at 45 °C. Then, the catalytic activity of such recycled **SM-Te** was determined except that **SM-Te** was replaced by the recycled **SM-Te**. Subsequently, the catalytic composition in the assay system was recycled once again using a similar method mentioned above, and the corresponding catalytic activity was determined once again. A similar recycling process and determination of catalytic activity were repeated for a total of three times. The catalytic rates are illustrated in Fig. 9.

Results and discussion

Construction of supramolecular microgel SM-Te

Commonly, ROS are harmless to humans and act as signal molecules in the metabolism. However, the overproduction of ROS can cause many human oxidative stress-related diseases. Therefore, in our previous report, a smart artificial GPx (**Microgel GPx**) with controllable catalytic activity was constructed based on the covalent bond crosslinked microgel (PNIPAM) scaffold, which was designed to endow **Microgel GPx** with the temperature responsive catalytic activity. It can potentially be used in the development of intelligent antioxidant drugs to adjust the appropriate concentration of ROS.[24] Although the successful construction of **Microgel GPx** highlights the development of intelligent antioxidant drugs, there are serious and insurmountable disadvantages in **Microgel GPx** related to its purification process and covalently crosslinked scaffold. Firstly, the efficient separation of CTAB from the microgel solution during the purification process was not achievable. Secondly, the covalently crosslinked microgel scaffold of **Microgel GPx** exhibited an average diameter of 160 nm.

And its molecular weight was far higher than that of the traditional single chain polymer. Therefore, **Microgel GPx** was difficult to be degraded or excreted by the metabolic system. These two disadvantages have largely limited the further application of **Microgel GPx**. Usually, the purity and productivity of the supramolecular microgel is desirable. Importantly, as the supramolecular microgel has the unique property of dynamic and reversible self-assembled behaviour, the artificial GPx based on the supramolecular microgel can be easily degraded under appropriate conditions. Therefore, **SM-Te** can be endowed with the advantages of the effective preparation process and potential degradable ability if **SM-Te** was constructed based on the supramolecular microgel scaffold. In other words, compared with previous **Microgel GPx**, **SM-Te** was more advantageous, the successful construction of which will overcome the two insurmountable disadvantages mentioned above. Herein, to construct the supramolecular scaffold of **SM-Te**, the corresponding supramolecular building block was designed. As shown in Fig. 1, the monomer NIPAM, acrylamide (**AM**), and **CD-monomer** were selected as functional monomers.

Herein, NIPAM endowed the scaffold of **SM-Te** with temperature responsive behaviour. **AM** functions as the hydrophilic block in the scaffold of **PPAM-CD**. It is known that the soluble PNIPAM can transform into an insoluble polymer when the temperature becomes higher than LCST. The soluble block copolymer bearing the PNIPAM block can transform into an amphiphilic polymer when the temperature becomes higher than LCST. Under these conditions, the controllable aggregated structures (micelles, vesicles, nanorods and so on) can be formed. Therefore, **AM** acted as the hydrophilic block in the amphiphilic **PPAM-CD** when the temperature was above the LCST, which provides the platform for the construction of **SM-Te**. The graphical representation of the self-assembly process (A–C) is shown in Scheme 1. The **CD-monomer** functions as the host molecule in **PPAM-CD**, which can be further employed to complex the guest molecule in the construction process of **SM-Te**. Considering that ATRP was an efficient technique for the synthesis of block copolymers with a controlled structure,[55,56] **PPAM-CD** was synthesized by ATRP and used as the building block for **SM-Te**. Additionally, the crystal structure of bovine erythrocyte GPx was reported by Epp *et al.* in 1983.[5] The catalytic active site of GPx has been well studied by mimicking the catalytic center of selenocysteine in GPx using tellurium-containing molecules.[17,32] It has been proved that tellurium-containing molecules act as more efficient scaffolds for artificial GPx compared with selenium-containing molecules. Therefore, the tellurium-containing guest molecule (**ADA-Te-ADA**) was synthesized, which served two purposes in **SM-Te:** one as an excellent alternative for selenocysteine in native GPx and the other one as a cross-linker for the construction of **SM-Te** based on the host–guest interaction. Additionally, **AZO** was employed as a competitive guest for the confirmation of the formation of the supramolecular microgel in the NMR assay.

As PNIPAM is a thermally sensitive polymer with a lower critical solution temperature (LCST) of 32 °C, it undergoes a reversible volume phase transition at near-physiological temperature.[57,58] Its polymer block shifts from being hydrophilic

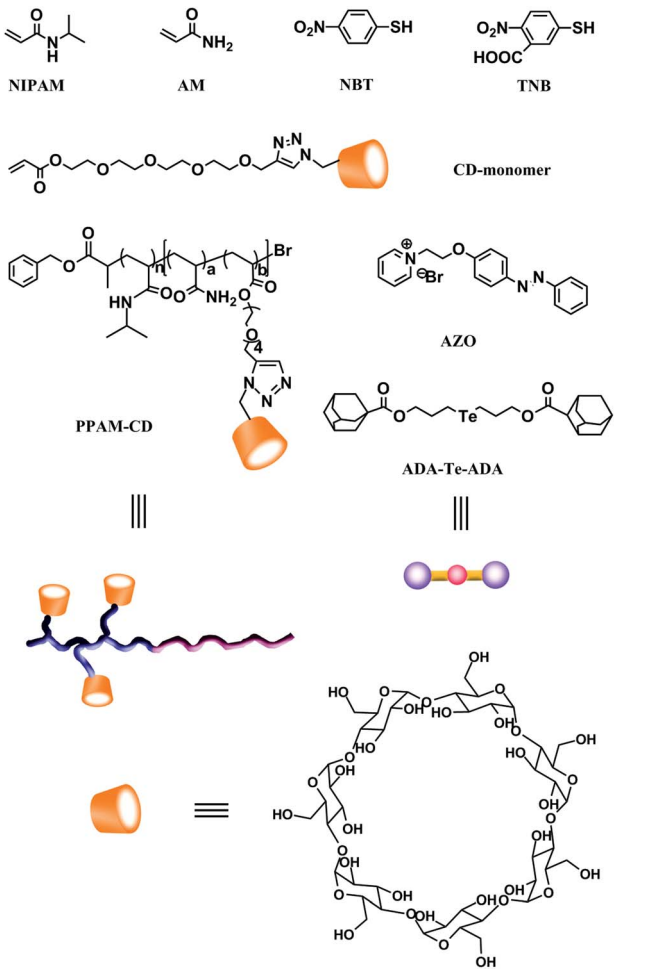

Fig. 1 The structures of the functional monomers NIPAM, AM, CD-comonomer, cyclodextrin-containing host block copolymer (PPAM-CD), tellurium-containing guest molecule (ADA-Te-ADA) and substrates (NBT, TNB).

to hydrophobic when the temperature was above the LCST. Therefore, the soluble block copolymer bearing the PNIPAM block can transform into an amphiphilic polymer when the temperature was above the LCST, which provides the platform for the construction of versatile self-assembled materials.[24,59,60] Benefitting from the temperature responsive properties of the PNIPAM scaffold, **Microgel GPx** exhibited the temperature responsive catalytic behaviour during the temperature responsive process of the PNIPAM scaffold. Herein, the temperature responsive properties of the PNIPAM scaffold in **PPAM-CD** were also employed in the construction of **SM-Te**, which might provide the basement for adjusting the catalytic activity of **SM-Te**. To provide the basic information for the construction of **SM-Te**, the temperature responsive properties of **PPAM-CD** were first investigated. The LCST of **PPAM-CD** was determined to be 34.4 °C (shown in Fig. 2a). The stable optical transmittance of **PPAM-CD** was observed when the temperature was higher than 35 °C.[20] Additionally, from Fig. 3a, the hydrodynamic diameter of **PPAM-CD** at 25 °C was less than 10 nm, which proved that **PPAM-CD** was soluble in water. However, the self-assembled

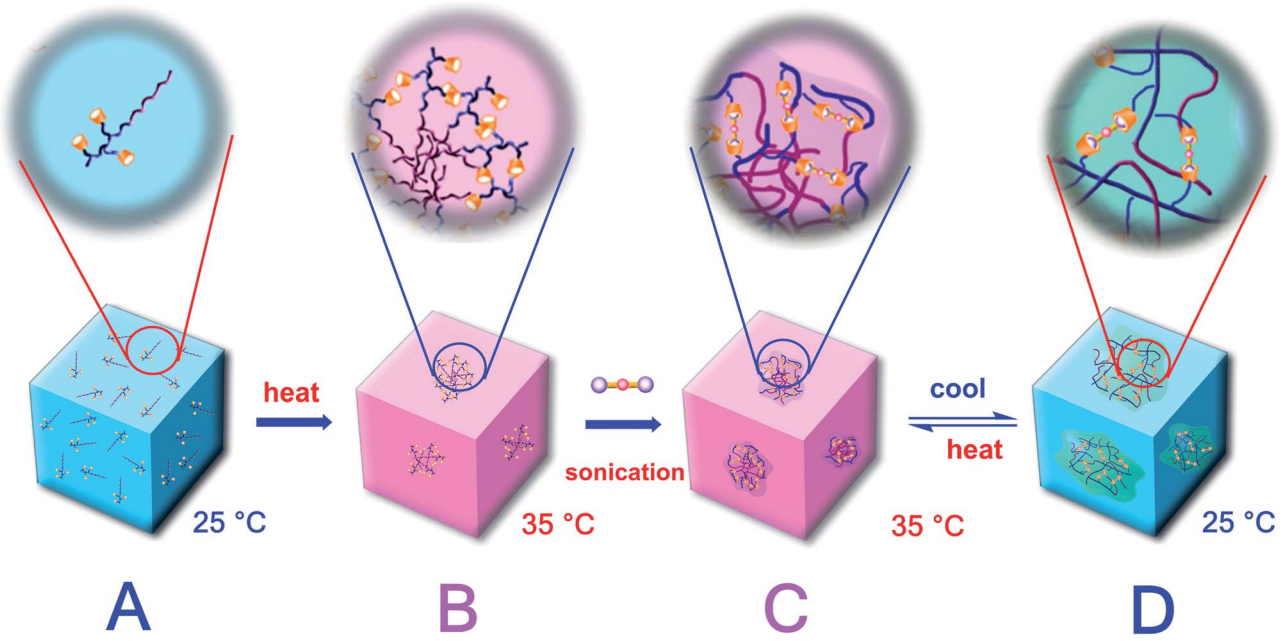

Scheme 1 A graphical representation of the self-assembled process (A–C) and the reversible responsive behaviour (C and D) of **SM-Te**.

aggregation with 230 nm (Fig. 3d) in hydrodynamic diameter was formed at 35 °C as **PPAM-CD** was transformed into an amphiphilic polymer. These observations indicated that the efficient self-assembled aggregation could be formed at 35 °C. Therefore, **SM-Te** was prepared at 35 °C and the graphical representation of the self-assembly process is given in Scheme 1. As illustrated in Scheme 1A, **PPAM-CD** was soluble at 25 °C. Then, as shown in Scheme 1B, the self-assembled aggregation was formed and the distance of cyclodextrins in **PPAM-CD** was decreased when the temperature was 35 °C which was higher than the LCST of **PPAM-CD**. Subsequently, the guest molecule **ADA-Te-ADA** was added into the above solution under sonication at 35 °C. Accordingly, the host–guest supramolecular complex in the network of **SM-Te** was formed between cyclodextrin in **PPAM-CD** and adamantane in **ADA-Te-ADA** (Scheme 1C). The confirmation of the formation of **SM-Te** is given in the following section.

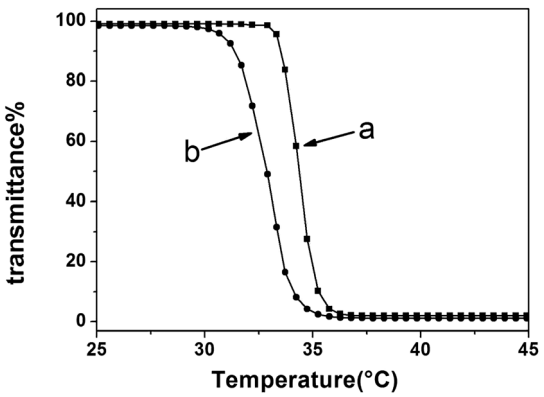

Fig. 2 Temperature dependence of optical transmittance at 600 nm obtained for solutions (pH = 7.0, 50 mM PBS) of (a) **PPAM-CD** and (b) **SM-Te** at concentrations of 1 mg mL^{-1}.

Characterization of supramolecular microgel SM-Te

The formation of the host–guest supramolecular complex in the network of **SM-Te** was confirmed by the change of optical transmittance, dynamic light scattering, NMR, SEM, and TEM. From Fig. 2, it can be found that the temperature dependence of optical transmittance of **SM-Te** (curve b) was different from that of **PPAM-CD** (curve a). The LCST of **SM-Te** was 32.8 °C, which was lower than that of **PPAM-CD** (34.4 °C). We supposed that two factors played roles in the decrease of LCST. On the one hand, the network of **SM-Te** was crosslinked by **ADA-Te-ADA**. The molecular morphology of **SM-Te** with a network structure was larger than that of **PPAM-CD** (the normal single chain polymer). It has been proved that the aqueous solution of PNIPAM showed a strong decrease of LCST with increasing molecular weight.[57,58] Therefore, the decreased LCST of **SM-Te** possibly resulted from that the molecular weight of **SM-Te** was higher than that of **PPAM-CD**. One the other hand, considering

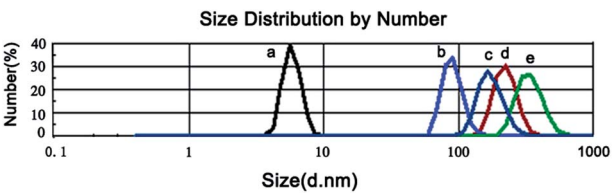

Fig. 3 Hydrodynamic diameters of **PPAM-CD** at varying temperatures (a, 25 °C; d, 35 °C) and hydrodynamic diameters of **SM-Te** at varying temperatures (b, 45 °C; c, 35 °C; e, 25 °C) determined using a Malvern ZETAS12-ERNANOSERIES instrument.

that **ADA-Te-ADA** was a hydrophobic molecule and acted as the crosslinker in **SM-Te**, **SM-Te** was anchored with more hydrophobic factors and might exhibit lower LCST. This phenomenon was in good agreement with a previous report.[61] Consequently, the difference of the LCSTs between **SM-Te** and **PPAM-CD** preliminarily proved that the self-assembled structure of **SM-Te** was formed. Additionally, comparing the temperature dependence of optical transmittance of **SM-Te** and **Microgel GPx**,[24] we found that they exhibited similar temperature responsive behaviour. Considering that the change of the structure can result in the change of catalytic activity of an artificial enzyme, similar temperature responsive behaviour of **SM-Te** and **Microgel GPx** might enable their catalytic activities exhibiting similar temperature responsive behaviour. The confirmation of this suspect is presented in the following section (Catalytic activity modulated by temperature).

To further prove the formation of the host–guest complex in **SM-Te**, NMR assay was employed using **AZO** as the competitive guest. Compared with the host–guest interaction between **AZO** and cyclodextrin, the host–guest interaction between **ADA-Te-ADA** and cyclodextrin was much stronger. The host–guest complex between **ADA-Te-ADA** and cyclodextrin was more stable. Therefore, we assumed that **ADA-Te-ADA** could supplant **AZO** from the cave of cyclodextrin even if the inclusion complexation had primarily formed between **AZO** and cyclodextrin. In other words, **AZO** could act as the indicator to confirm the host–guest complex between **ADA-Te-ADA** and cyclodextrin. The graphical representation of the competitive complex mechanism using **AZO** as an indicator is shown in Scheme 2.

To confirm this hypothesis, three groups of ^{1}H NMR spectra are characterized and illustrated in Fig. 4. Among three groups of ^{1}H NMR spectra, Fig. 4A provides the proton signals of aromatic rings in pure **AZO**, Fig. 4B provides the proton signals of aromatic rings in the binary system of **AZO**/cyclodextrin, and Fig. 4C provides the proton signals of aromatic rings in the ternary system of **AZO**/cyclodextrin/**ADA-Te-ADA**. Comparing Fig. 4B with Fig. 4A, we noticed that proton signals of c_2, a_2, b_2, h_2 shifted to a low field, which suggested that these protons in the binary system were exposed to water moderately and were not included by cyclodextrin. We also found that proton signals

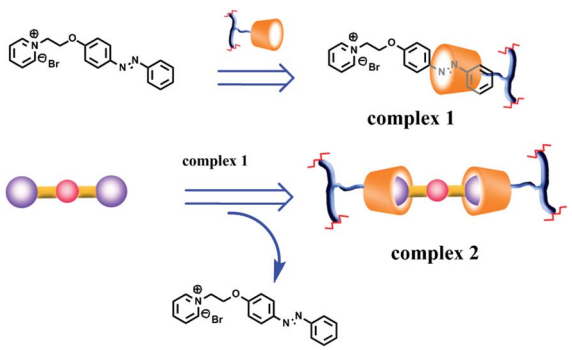

Scheme 2 A graphical representation of the competitive complex mechanism using AZO as an indicator.

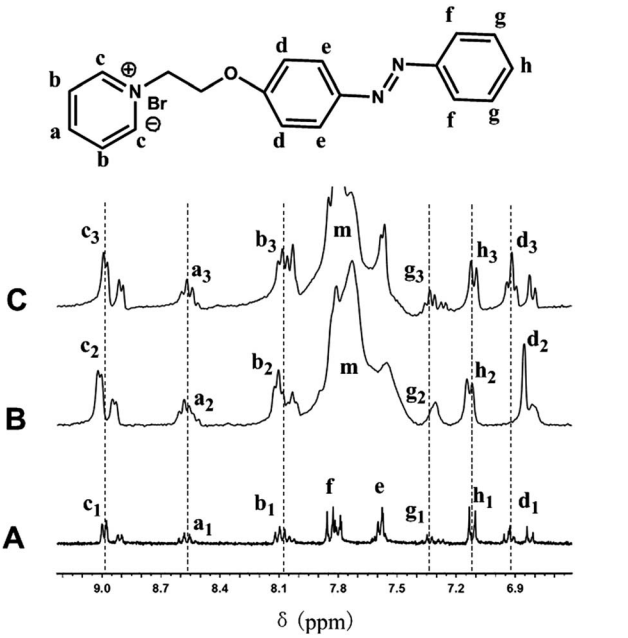

Fig. 4 ^{1}H NMR spectra of (A) the proton signals of aromatic rings in pure AZO, (B) the proton signals of aromatic rings in the binary system of AZO/cyclodextrin, and (C) the proton signals of aromatic rings in the ternary system of AZO/cyclodextrin/ADA-Te-ADA in D_2O.

of d_2 and g_2 shifted to a high field (proton signals of e_2 and f_2 were buried by the protons of the polymer), which suggested that these protons were included in the hydrophobic cavity of cyclodextrin and the proton signals were shielded. These results were in line with the previous report that investigated the formation mechanism of the host–guest complex between **AZO** and functional cyclodextrin.[62] Moreover, proton signals of d_2 and g_2 were broad peaks compared with d_1 and g_1, which also proved that these protons were included in the hydrophobic cavity of cyclodextrin. A similar result was also reported previously.[63] Subsequently, a ternary system of **AZO**/cyclodextrin/**ADA-Te-ADA** was obtained by adding **ADA-Te-ADA** into the above binary system of **AZO**/cyclodextrin (as shown in Fig. 4C). It was noticeable that the proton signals of aromatic rings in the ternary system were the same as that of pure **AZO**, which suggested that the **AZO** was not included in the cavity of cyclodextrin and the complex of **AZO**/cyclodextrin was not formed. Equally, it confirmed the hypothesis that **ADA-Te-ADA** could supplant **AZO** from the cave of cyclodextrin and the complex of **ADA-Te-ADA**/cyclodextrin was indeed formed.

As the supramolecular microgel was used as the scaffold for **SM-Te**, it was necessary to reveal the detailed information of the aggregation morphology that was essential for the investigation of the catalytic mechanism of artificial GPx. Firstly, dynamic light scattering was employed to explore the temperature dependence of the hydrodynamic diameter of **SM-Te**. As shown in Fig. 3, the hydrodynamic diameters of **SM-Te** at 25 °C (curve e), 35 °C (curve c), and 45 °C (curve b) were 360 nm, 190 nm, and 98 nm, respectively. Especially, it was noticeable that the hydrodynamic diameter of **SM-Te** (Fig. 3e) at 25 °C (below the LCST of 32.8 °C) was strikingly different from that of **PPAM-CD**

(Fig. 3a) under the same conditions. The difference in the diameters was possibly derived from the different molecular morphologies of **SM-Te** and **PPAM-CD**. It further proved that the crosslinked supramolecular microgel with a larger hydrodynamic diameter was formed. Additionally, the hydrodynamic diameter was decreased with the increase of temperature from 35 °C to 45 °C, which might be caused by the reason that PNIPAM in **SM-Te** became more hydrophobic and the network scaffold of **SM-Te** was contracted at higher temperatures. Commonly, the change of the hydrophobicity of PNIPAM was caused by the break of hydrogen bonds between the amide group of PNIPAM and the surrounding water. For naturally occurring enzymes, abundant studies indicated that a minor change of the structure of the enzyme would result in a dramatic change in catalytic activity. Herein, the temperature responsive changes of the hydrophobic diameter of **SM-Te** provided important insight into the regulation of the catalytic activity of smart artificial GPx.

Furthermore, the actual morphology of **SM-Te** when the temperature was higher than its LCST was observed by SEM (as shown in Fig. 5). From the SEM image, we clearly found that the presence of spherical nanoparticles of about 80 nm in average diameter. The dimensions of the nanoparticles observed from SEM were smaller than those obtained from dynamic light scattering. This phenomenon might be derived from the reason that the zetasizer nano-instrument reported the average hydrophobic diameter with the contribution of a swollen corona of nanoparticles. To further reveal the detailed morphologies of the spherical nanoparticles, their structures were observed by TEM (as shown in Fig. 6). It was apparent that the diameters of spherical nanoparticles were 70–80 nm, which was in close agreement with the SEM assay. Particularly, many tiny holes were observed in the spherical nanoparticles, which was the typical character of a microgel. In our previous report, the nanoparticles assembled by **PPAM-CD** were hollow vesicle-like nanoparticles with a thinner region surrounded by a thicker region.[20] Herein, the unique structure of **SM-Te** observed by TEM further proved that the supramolecular microgel was indeed prepared.

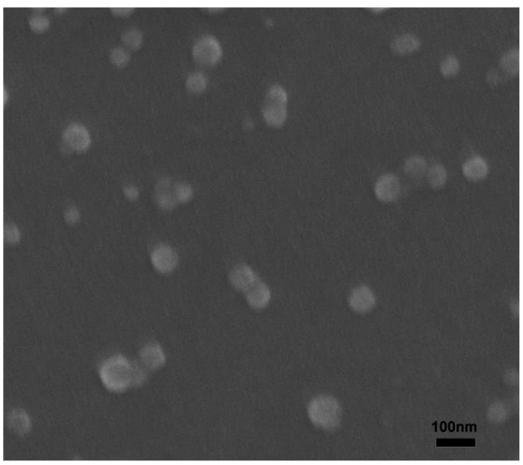

Fig. 5 SEM image of SM-Te.

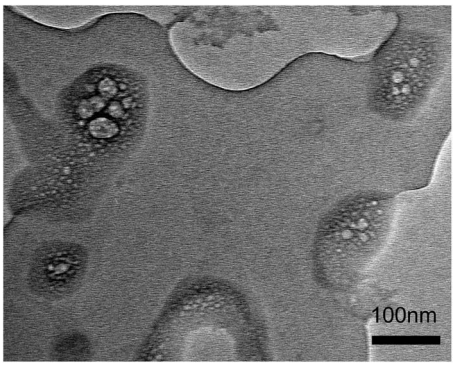

Fig. 6 TEM image of SM-Te.

Consequently, all the results based on optical transmittance, dynamic light scattering, NMR, SEM, and TEM indicated that the supramolecular microgel **SM-Te** was successfully constructed. Additionally, comparing the detailed information of the structure of **SM-Te** mentioned above and that of **Microgel GPx**,[24] we concluded that they exhibited similar nano-scaled aggregated structures. It is known that a slight change of the structure will result in a dramatic change in catalytic activity of a successful artificial enzyme. Considering that **SM-Te** and **Microgel GPx** exhibited the structures with a similar aggregated scale, we anticipated that they might be endowed with similar catalytic behaviour. The confirmation of this suspect is presented in the following section (Catalytic behaviour of supramolecular microgel **SM-Te**).

Finally, the graphical representations of the self-assembled process of **SM-Te** (Scheme 1A–C) and the reversible responsive behaviour of **SM-Te** (Scheme 1C and D) are illustrated.

Catalytic behaviour of supramolecular microgel SM-Te

Herein, for evaluating the catalytic behaviour of **SM-Te**, the catalytic activity of **SM-Te** for the reduction of cumene hydroperoxide (CUOOH) by TNB (3-carboxyl-4-nitrobenzenethiol) was determined according to a modified method reported by Hilvert *et al.*[6] using TNB as a GSH alternative (see Fig. 7). The activity was given assuming one molecule catalytic center (Te-monomer) in **SM-Te** as one active site of the enzyme. The reaction was initiated by the subsequent addition of hydroperoxide, and the absorbance at 410 nm ($\varepsilon_{410} = 13\,600\ M^{-1}\ cm^{-1}$, pH = 7.0) was recorded for a few minutes to calculate the reaction rate. The relative activities are summarized in Table 1.

To investigate the temperature responsive properties of **SM-Te**, the catalytic activity was determined in the TNB assay system using CUOOH as the substrate at various temperatures

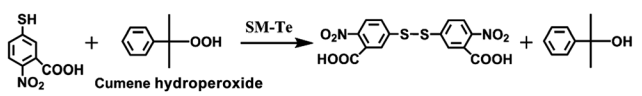

Fig. 7 Determination of the GPx catalytic rate for the reduction of cumene hydroperoxide (CUOOH) using TNB (3-carboxyl-4-nitrobenzenethiol) as the substrate.

from 25 °C to 45 °C (as shown in Table 1). To the best of our knowledge, for the majority of temperature-activated reactions, the reaction rates will enhance with the rising temperature according to the Arrhenius equation. However, it was different for **SM-Te**. To vividly present the temperature responsive behaviour of **SM-Te**, a bell shaped thermally responsive catalytic activity curve was obtained by plotting the catalytic reaction rates against temperatures (Fig. 8). It was observed that the catalytic rate increased slowly with increasing temperature when the temperature was lower than 32 °C, and it increased largely with the increase of the temperature from 32 °C to 38 °C. Nevertheless, it was noticeable that the catalytic activity decreased sharply when the temperature was further increased above 38 °C. Similarly, for the temperature responsive behaviour of **Microgel GPx**,[24] a bell shaped curve was also obtained by plotting the catalytic rates against temperature. Contrastively, the highest catalytic rate was obtained at 32 °C for **Microgel GPx**. However, the highest catalytic rate was obtained at 38 °C for **SM-Te**. Significantly, the temperature of 38 °C (related to the highest catalytic rate of **SM-Te**) was close to the physiological temperature compared with 32 °C (related to the highest catalytic rate of **Microgel GPx**). Therefore, considering that the temperature of the highest catalytic rate of **SM-Te** was close to the physiological temperature, **SM-Te** was superior to **Microgel GPx** when it was used to develop intelligent antioxidant drugs. Especially, for **SM-Te**, the highest catalytic rate was obtained at higher temperature, which might be derived from the stronger hydrophilicity of the **SM-Te** scaffold as the hydrophilic cyclodextrin was anchored. Herein, for the temperature responsive catalytic behaviour of **SM-Te**, we speculated that such a phenomenon was derived from the changes of the hydrophobic microenvironment and pore size of the supramolecular microgel network by altering the temperature. The confirmation of this suspect is presented in the following section (Catalytic activity modulated by temperature).

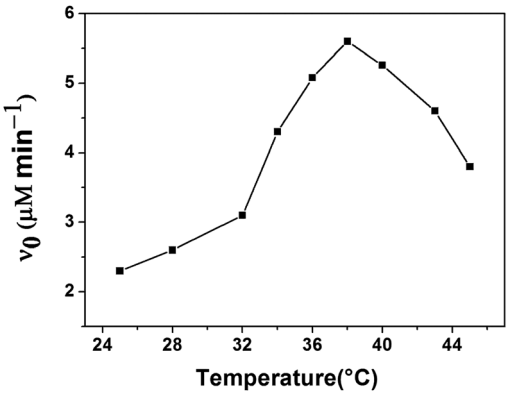

Fig. 8 Plots of the catalytic rates of SM-Te *versus* temperatures during the catalytic reduction of CUOOH (0.25 mM) by TNB (0.15 mM) and a catalytic center (1.00 μM).

Table 1 The initial rates (v_0) and activities for the reduction of hydroperoxides (250 μM) by TNB (150 μM) in the presence of SM-Te at pH 7.0 (50 mM PBS) and 36 °C

Number	Catalyst	Temperature (°C)	ArSH	ROOH	v_0[a] (mM min^{-1})
1	**SM-Te**	25	TNB	CUOOH	2.31
2	**SM-Te**	28	TNB	CUOOH	2.60
3	**SM-Te**	32	TNB	CUOOH	3.12
4	**SM-Te**	34	TNB	CUOOH	4.32
5	**SM-Te**	36	TNB	CUOOH	5.08
6	**SM-Te**	38	TNB	CUOOH	5.60
7	**SM-Te**	40	TNB	CUOOH	5.26
8	**SM-Te**	43	TNB	CUOOH	4.63
9	**SM-Te**	45	TNB	CUOOH	3.82
10	**Microgel GPx**[b]	38	TNB	CUOOH	3.94
11	**PhSeSePh**	38	TNB	CUOOH	0.011
12	**SM-Te**	38	TNB	H_2O_2	0.86
13	**SM-Te**	38	NBT	CUOOH	6.25
14	**SM-Te**	38	NBT	H_2O_2	1.28

[a] The initial rate of reaction was corrected for the spontaneous oxidation. And the concentration of the catalyst is 1 μM and assuming one molecule catalytic center (tellurium moiety) as one active site of the enzyme. [b] The covalent bond crosslinked microgel artificial GPx constructed in our previous report.[24]

Moreover, as a catalyst, the investigation of the stability of the composition of **SM-Te** prior to reaction and after reaction is really important. It is essential to the further investigation and application of **SM-Te**. It is known that a slight change of the structure will result in a dramatic change in the catalytic activity of an artificial enzyme and a native enzyme. In other words, **SM-Te** will exhibit a large change in catalytic activity if its composition has changed. Therefore, considering that the catalytic activity was crucially important for a successful artificial GPx, we chose the data of the catalytic activity as the effective values to evaluate the stability of the composition of **SM-Te**. Herein, to achieve this aim, we designed an experiment (see Investigation of the stability of **SM-Te** in the Experimental section). And the catalytic activity of **SM-Te**, recycled **SM-Te** for one time, recycled **SM-Te** for two times, and recycled **SM-Te** for three times was 5.56 μM min^{-1}, 5.49 μM min^{-1}, 5.44 μM min^{-1}, and 5.32 μM min^{-1}, respectively. And the vivid histogram of catalytic rates is illustrated in Fig. 9. By analysis of these catalytic rates, we found that the catalytic activities were slightly changed during the recycled process. Considering that a slight change of the structure would result in a dramatic change in the catalytic activity of an artificial enzyme, the slight change of catalytic activity indirectly proved that the composition of **SM-Te** was stable under the reaction conditions and the recycled process of **SM-Te**. Equally, it has been proved that the composition of **SM-Te** was stable and remained the same prior to reaction and after reaction.

Commonly, the catalytic rate of the background (nonenzymatic) reaction between CUOOH and TNB at 38 °C was very slow. As shown in Table 1, a slight enhancement in the catalytic rate was observed (v_0 = 0.011 μM min^{-1}) when the traditional small molecule artificial GPx (PhSeSePh) was used under the identical conditions. Amazingly, **SM-Te** constructed in this work exhibited a remarkable rate enhancement (v_0 = 5.60 μM min^{-1}). Compared with the catalytic rate of previous **Microgel GPx** (see Table 1, v_0 = 3.94 μM min^{-1}) determined under the same conditions, **SM-Te** exhibited higher catalytic activity. Additionally, considering that

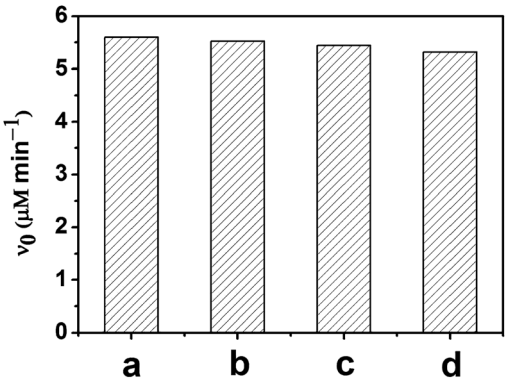

Fig. 9 The initial rates (v_0) for the reduction of CUOOH (250 μM) by TNB (150 μM) in the presence of **SM-Te** (a) and recycled **SM-Te** (b: recycled for one time; c: recycled for two times; d: recycled for three times).

SM-Te can overcome the insurmountable disadvantages existed in previous microgel artificial GPx, **SM-Te** was satisfactory as a novel and excellent smart artificial GPx. Moreover, as shown in Fig. 10, the saturation kinetics behaviour of **SM-Te** for the peroxidase reaction were studied at the individual concentrations of CUOOH, which indicated that **SM-Te** exhibited typical saturation kinetics behaviour and acted as a real catalyst for the peroxidase reaction. In the TNB assay system, the apparent kinetic parameters were obtained as follows: $V_{max} = 16.32$ μM min^{-1}, $k_{cat}^{app} = 16.32$ min^{-1}, $K_{m\ CUOOH} = 418.01$ μM and $k_{cat}^{app}/K_{m\ CUOOH} = 3.90 \times 10^4$ M^{-1} min^{-1}, and the turnover number per catalytic center tellurium was calculated to be 16 min^{-1}. Comparing the apparent kinetic parameters of **SM-Te** mentioned above and that of **Microgel GPx**,[24] similar saturation kinetics behaviour was observed. The similarity of saturation kinetics behaviour might be derived from similar aggregated structures and similar temperature responsive behaviour of their scaffolds. Although **SM-Te** and **Microgel GPx** exhibited similar adjustable catalytic activity and saturation kinetics behaviour, **SM-Te** was endowed with additional advantages of effective preparation process and potential degradable ability. Therefore, **SM-Te** was a more excellent scaffold for the development of intelligent antioxidant drugs.

Catalytic activity modulated by temperature

As shown in Fig. 8, **SM-Te** exhibited typical temperature responsive catalytic behaviour. Herein, **ADA-Te-ADA** was anchored with the GPx catalytic center (tellurium) and acted as the crosslinker for the supramolecular microgel network. In our previous work, the covalent bond crosslinker with the GPx catalytic center was employed, which was anchored into the microgel scaffold of **Microgel GPx**.[24] It was proved that the change of the pore size of microgel networks of **Microgel GPx**, the change of the hydrophobic microenvironment, and the shrinkage of **Microgel GPx** play important roles in adjusting the catalytic activity. Considering that **SM-Te** and **Microgel GPx** were constructed based on a similar PNIPAM scaffold, the shrinkage of a PNIPAM scaffold would result in the pore size of a supramolecular microgel becoming smaller. It might further result in the changes of the substrate binding ability and catalytic activity. Thus, we speculated that the temperature responsive catalytic behaviour of **SM-Te** was endowed from the changes of the hydrophobic microenvironment and pore size of the supramolecular microgel network. The graphical representation of responsive behaviour of the supramolecular microgel network in **SM-Te** is illustrated in Scheme 1C and D. To explicate the temperature responsive catalytic mechanism, optical transmittance, dynamic light scattering and catalytic rates measured in different assay systems were employed.

Based on the change of optical transmittance with increasing temperature mentioned in Fig. 2b, we noticed that the optical transmittance of **SM-Te** was stable (below 2%) when the temperature was above 35 °C. It meant that the efficient self-assembled aggregation was formed above 35 °C, which was resulted from the thermal sensitive properties of the PNIPAN scaffold in **SM-Te**. Commonly, the hydrophobic microenvironment could be formed in the self-assembled aggregation when the temperature was above the LCST of PNIPAN. Significantly, the hydrophobic microenvironment is one of the pivotal catalytic factors that contribute to maintain efficient GPx catalytic activity.[19,24] Herein, this crucial role of the hydrophobic microenvironment was reflected by the remarkably enhanced catalytic rates when the temperature increased from 32 °C to 38 °C.

Moreover, we proved that the pore size existed in a covalent bond network of **Microgel GPx** played an important role in altering the catalytic rates.[24] Similarly, this phenomenon was also observed in **SM-Te**. Combining the change of hydrodynamic diameter with increasing temperature as shown in Fig. 3 and the change of catalytic rate with increasing temperature as shown in Fig. 8, we found that the catalytic rates could be adjusted according to the change of hydrodynamic diameter. Typically, the hydrodynamic diameter was about 360 nm when the temperature was 25 °C (below the LCST of 32.8 °C). Under these conditions, the microgel scaffold of **SM-Te** was swelling, the optical transmittance was near 100%, the pore size of **SM-Te** was larger, and the hydrophobic microenvironment was not formed. Therefore, the pivotal catalytic factor was absent, which

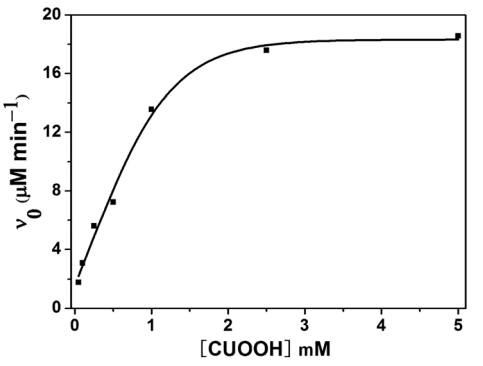

Fig. 10 Plots of initial rates at different concentrations of CUOOH in the presence of **SM-Te**. The initial concentration of TNB was fixed to 0.15 mM. The concentrations of CUOOH were 0.05, 0.10, 0.25, 0.5, 1, 2.5 and 5 mM, respectively.

further resulted in the weak substrate binding ability and low catalytic rate. Subsequently, the microgel scaffold of **SM-Te** was deswelling when the temperature was 35 °C (above the LCST of 32.8 °C). The hydrodynamic diameter was about 190 nm, the optical transmittance was below 2%, the pore size of **SM-Te** was contracted, and the hydrophobic microenvironment was preliminarily formed. As the pivotal catalytic factor that contributes to maintain efficient GPx catalytic activity was presented, the substrate binding ability and catalytic rate were remarkably enhanced under these conditions. However, as shown in Fig. 8, it was noticeable that the catalytic activity decreased sharply when the temperature continuously increased above 38 °C. Typically, under these conditions at 45 °C, the hydrodynamic diameter was about 98 nm, the hydrophobicity of the PNIPAM scaffold was further increased, and the pore sizes in **SM-Te** were further contracted, which were not suitable for allowing substrates to permeate into the cores of **SM-Te** and finish the GPx catalytic reaction. Therefore, the catalytic rate was sharply decreased under these conditions as the efficient binding ability for substrates could not be achieved. These observations proved that the changes of the hydrophobic microenvironment and pore size indeed played important roles in regulating the GPx catalytic rates. A similar temperature responsive catalytic mechanism was also investigated for **Microgel GPx**.[24]

Additionally, the maximum catalytic rate was obtained at 38 °C. The catalytic rates obtained at 35 °C (the optical transmittance was just stable) and at LCST of **SM-Te** were all lower than the maximum catalytic rate. It was because that the optimum substrate binding ability was not achieved below 38 °C even if the hydrophobic microenvironment and pore size are maintained to some extent under these conditions.

To further confirm that changes of the hydrophobic microenvironment and pore size of the supramolecular microgel network played important roles in adjusting the temperature responsive catalytic rates. The catalytic reactions were measured in different assay systems using various substrates with different hydrophobic abilities and molecule sizes (CUOOH, TNB assay system (Fig. 11A), $v_0 = 5.60$ μM min^{-1}; CUOOH, NBT assay system (Fig. 11B), $v_0 = 6.25$ μM min^{-1}; H_2O_2, TNB assay system (Fig. 11C), $v_0 = 1.28$ μM min^{-1}; H_2O_2, NBT assay system (Fig. 11A), $v_0 = 0.86$ μM min^{-1}). The difference between NBT and TNB was that NBT was a smaller molecule in size than TNB owing to the lack of a carboxyl functional group in NBT. The difference between CUOOH and H_2O_2 was that CUOOH was a more hydrophobic substrate than H_2O_2 owing to the presence of the hydrophobic cumenyl group in CUOOH.

Firstly, under the identical conditions at 38 °C, we found that the higher catalytic rate was observed when NBT was used as the substrate (as shown in Fig. 11, A < B, or C < D). Considering that the hydrophobic microenvironment has formed and the pore size has contracted at 38 °C, a dramatic change in the catalytic rate in different assay systems using TNB or NBT as the substrate was anticipated. It should be caused by the shrinkage of the pore size in the network of **SM-Te** that made TNB not easily permeate into the cores of **SM-Te** and finish the GPx catalytic reaction. Whereas the NBT with a smaller size could still permeate into the core to finish the GPx catalytic reaction, and the higher catalytic activity was obtained. This phenomenon suggested that the effect of pore size was vital for adjusting the catalytic behaviour. Secondly, we also found that the higher catalytic rate was observed when CUOOH was used as the substrate (as shown in Fig. 11, A > C, or B > D). Commonly, the rate constants of the spontaneous reaction between hydroperoxide and thiol vary in magnitude in the order $k(H_2O_2) > k(\text{CUOOH})$.[12] Nevertheless, it was noticeable that the higher catalytic rate was observed when CUOOH was used as the substrate for **SM-Te** at 38 °C. Typically, the difference between CUOOH and H_2O_2 was that CUOOH was a more hydrophobic substrate than H_2O_2 owing to the presence of the hydrophobic cumenyl group in CUOOH. The difference in the catalytic rate in different assay systems (the different activity for CUOOH and H_2O_2) was mainly because that the hydrophobic microenvironment enabled the hydrophobic substrate CUOOH to approach the catalytic center (tellurium in **ADA-Te-ADA**) efficiently and complete the catalytic cycle more preferentially. It was proved that the different structure of CUOOH and H_2O_2 played an important role in different activities. Additionally, this observation also proved that hydrophobic microenvironment in **SM-Te** also played an important role in adjusting the temperature responsive catalytic behaviour.

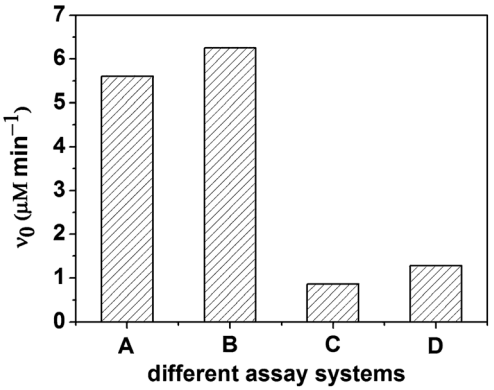

Fig. 11 The initial rates (v_0) for the reduction of hydroperoxide (250 μM) by thiol TNB or NBT (150 μM) in the presence of **SM-Te** at pH 7.0 (50 mM PBS) and 38 °C: (A) CUOOH, TNB; (B) CUOOH, NBT; (C) H_2O_2, TNB; (D) H_2O_2, NBT.

Therefore, based on the discussions mentioned above, we could draw a conclusion that both the changes of the hydrophobic microenvironment and pore size in the supramolecular microgel network of **SM-Te** played significant roles in adjusting the temperature responsive catalytic behaviour. **SM-Te** and **Microgel GPx** exhibited similar temperature responsive catalytic activity and saturation kinetics behaviour. Especially, **SM-Te** exhibited a higher catalytic rate than **Microgel GPx** under the same conditions at 38 °C (nearing the physiological temperature). Significantly, **SM-Te** was endowed with the advantages of effective preparation process and potential degradable ability, which could overcome the two insurmountable disadvantages of **Microgel GPx**. Considering that **SM-Te** exhibited such unique advantages compared with **Microgel GPx**, **SM-Te** was a satisfactory artificial GPx and

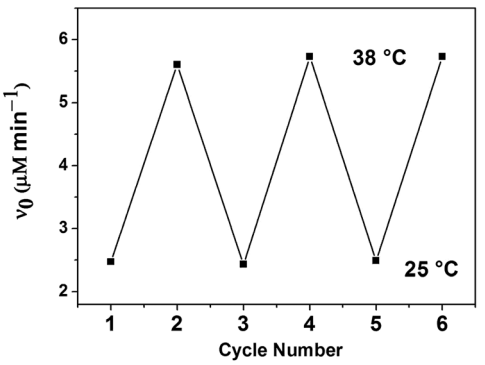

Fig. 12 Changes of the catalytic rates of SM-Te during heating–cooling cycles between 25 °C and 38 °C.

might act as a more excellent scaffold for the development of intelligent antioxidant drugs.

Ultimately, as a smart artificial GPx, the reversibility of the catalytic rates has been determined between 25 °C and 38 °C. As shown in Fig. 12, the catalytic rate of **SM-Te** was still maintained after several cycles of heating and cooling. The catalytic activity of **SM-Te** was completely reversible after multiple heating–cooling cycles.

Conclusions

In this work, the construction of a smart artificial GPx based on supramolecular microgels was carried out. The tellurium-containing guest molecule (**ADA-Te-ADA**) and the cyclodextrin-containing host block copolymer (**PPAM-CD**) were synthesized. And they were used as building blocks for the construction of **SM-Te** based on the host–guest interaction. Similar to the temperature responsive behaviour of PNIPAM, **SM-Te** also exhibited the typical temperature responsive behaviour. Moreover, the GPx catalytic behaviour of **SM-Te** displayed a noticeable temperature responsive characteristic and it also exhibited the typical saturation kinetics behaviour as a real enzyme catalyst. It was proved that the changes of the hydrophobic microenvironment and pore size in the supramolecular microgel network of **SM-Te** played significant roles in adjusting the temperature responsive catalytic behaviour. The successful construction of **SM-Te** not only overcomes the insurmountable disadvantages existed in **Microgel GPx** but also bodes well for the development of novel intelligent antioxidant drugs. The preparation method for the host–guest supramolecular microgel can also highlight the exploration of other novel host–guest self-assembled supramolecular materials.

Acknowledgements

This research was supported by the Guangxi Experiment Centre of Science and Technology (no. LGZXKF201106).

Notes and references

1 H. Sies, *Exp. Physiol.*, 1997, **82**, 291–295.
2 H. Sies, Oxidative Stress: Introductory Remarks, in *Oxidative Stress*, ed. H. Sies, Academic Press, London, 1985, p. 1.
3 H. Sies, *Angew. Chem., Int. Ed. Engl.*, 1986, **25**, 1058–1071.
4 L. Flohé, G. Loschen, W. A. Günzler and E. Eichele, *Hoppe-Seyler's Z. Physiol. Chem.*, 1972, **353**, 987–999.
5 O. Epp, R. Ladenstein and A. Wendel, *Eur. J. Biochem.*, 1983, **133**, 51–69.
6 Z. P. Wu and D. Hilvert, *J. Am. Chem. Soc.*, 1990, **112**, 5647–5648.
7 L. Engman, D. Stern, I. A. Cotgreave and C. M. Andersson, *J. Am. Chem. Soc.*, 1992, **114**, 9737–9743.
8 T. Kanda, L. Engman, I. A. Cotgreave and G. Powis, *J. Org. Chem.*, 1999, **64**, 8161–8169.
9 J. Q. Liu, G. M. Luo, S. J. Gao, K. Zhang, X. F. Chen and J. C. Shen, *Chem. Commun.*, 1999, 199–200.
10 G. Mugesh and H. B. Singh, *Chem. Soc. Rev.*, 2000, **29**, 347–357.
11 T. G. Back and Z. Moussa, *J. Am. Chem. Soc.*, 2003, **125**, 13455–13460.
12 Z. Y. Dong, J. Q. Liu, S. Z. Mao, X. Huang, B. Yang, X. J. Ren, G. M. Luo and J. C. Shen, *J. Am. Chem. Soc.*, 2004, **126**, 16395–16404.
13 X. Huang, Y. Z. Yin, Y. Liu, X. L. Bai, Z. M. Zhang, J. Y. Xu, J. C. Shen and J. Q. Liu, *Biosens. Bioelectron.*, 2009, **25**, 657–660.
14 X. Huang, Y. Z. Yin and J. Q. Liu, *Macromol. Biosci.*, 2010, **10**, 1385–1396.
15 Z. Y. Dong, Q. Luo and J. Q. Liu, *Chem. Soc. Rev.*, 2012, **41**, 7890–7908.
16 C. X. Hou, Q. Luo, J. Q. Liu, L. Miao, C. Q. Zhang, Y. Z. Gao, X. Y. Zhang, J. Y. Xu, Z. Y. Dong and J. Q. Liu, *ACS Nano*, 2012, **6**, 8692–8701.
17 X. Huang, Y. Z. Yin, X. Jiang, Y. Tang, J. Y. Xu, J. Q. Liu and J. C. Shen, *Macromol. Biosci.*, 2009, **9**, 1202–1210.
18 S. J. Yu, Y. Z. Yin, J. Y. Zhu, X. Huang, Q. Luo, J. Y. Xu, J. C. Shen and J. Q. Liu, *Soft Matter*, 2010, **6**, 5342–5350.
19 Y. Z. Yin, X. Huang, C. Y. Lv, L. Wang, S. J. Yu, Q. Luo, J. Y. Xu and J. Q. Liu, *Macromol. Biosci.*, 2010, **10**, 1505–1516.
20 Y. Z. Yin, L. Wang, H. Y. Jin, C. Y. Lv, S. J. Yu, X. Huang, Q. Luo, J. Y. Xu and J. Q. Liu, *Soft Matter*, 2011, **7**, 2521–2529.
21 H. Staudinger and E. Husemann, *Ber. Dtsch. Chem. Ges. A/B*, 1935, **68**, 1618–1634.
22 A. Biffis, N. B. Graham, G. Siedlaczek, S. Stalberg and G. Wulff, *Macromol. Chem. Phys.*, 2001, **202**, 163–171.
23 Y. Z. Yin, Z. Y. Dong, Q. Luo and J. Q. Liu, *Prog. Polym. Sci.*, 2012, **37**, 1476–1509.
24 X. Huang, Y. Z. Yin, Y. Tang, X. L. Bai, Z. M. Zhang, J. Y. Xu, J. Q. Liu and J. C. Shen, *Soft Matter*, 2009, **5**, 1905–1911.
25 S. Lally, R. Liu, C. Supasuteekul, B. R. Saunders and T. Freemont, *J. Mater. Chem.*, 2011, **21**, 17719–17728.
26 R. A. Siegel, Y. Gu, M. Lei, A. Baldi, E. E. Nuxoll and B. Ziaie, *J. Controlled Release*, 2010, **141**, 303–313.
27 J. Gu, F. Xia, Y. Wu, X. Qu, Z. Yang and L. Jiang, *J. Controlled Release*, 2007, **117**, 396–402.
28 Y. Z. Gao, C. X. Hou, L. P. Zhou, D. M. Zhang, C. Q. Zhang, L. Miao, L. Wang, Z. Y. Dong, Q. Luo and J. Q. Liu, *Macromol. Biosci.*, 2013, **13**, 808–816.

29 S. Wiese, A. C. Spiess and W. Richtering, *Angew. Chem.*, 2013, **125**, 604–607.
30 B. Jimenez, A. Noyola, B. Capdeville, M. Roustan and G. Faup, *Water Res.*, 1988, **22**, 1253–1257.
31 L. E. Bromberg and E. S. Ron, *Adv. Drug Delivery Rev.*, 1998, **31**, 197–221.
32 A. Vila, A. Sánchez, K. Janes, I. Behrens, T. Kissel, J. L. V. Jato and M. a. J. Alonso, *Eur. J. Pharm. Biopharm.*, 2004, **57**, 123–131.
33 C. J. Pedersen, *J. Am. Chem. Soc.*, 1970, **92**, 386–391.
34 D. J. Cram and J. M. Cram, *Acc. Chem. Res.*, 1978, **11**, 8–14.
35 J. M. Lehn, *Science*, 1985, **227**, 849–856.
36 J. Araki and K. Ito, *Soft Matter*, 2007, **3**, 1456.
37 H. J. Kim, T. Kim and M. Lee, *Acc. Chem. Res.*, 2010, **44**, 72–82.
38 K. L. Liu, Z. Zhang and J. Li, *Soft Matter*, 2011, **7**, 11290.
39 J.-M. Lehn, *Chem. Soc. Rev.*, 2007, **36**, 151–160.
40 T. Ogoshi, Y. Takashima, H. Yamaguchi and A. Harada, *J. Am. Chem. Soc.*, 2007, **129**, 4878–4879.
41 I. Yoshimura, Y. Miyahara, N. Kasagi, H. Yamane, A. Ojida and I. Hamachi, *J. Am. Chem. Soc.*, 2004, **126**, 12204–12205.
42 M. Ikeda, R. Ochi and I. Hamachi, *Lab Chip*, 2010, **10**, 3325–3334.
43 J. Li, X. Li, X. Ni, X. Wang, H. Li and K. W. Leong, *Biomaterials*, 2006, **27**, 4132–4140.
44 J. Yu, H. Fan, J. Huang and J. Chen, *Soft Matter*, 2011, **7**, 7386.
45 Q. Wang, Z. Yang, X. Zhang, X. Xiao, C. K. Chang and B. Xu, *Angew. Chem., Int. Ed.*, 2007, **46**, 4285–4289.
46 Q. Wang, Z. Yang, M. Ma, C. K. Chang and B. Xu, *Chem. – Eur. J.*, 2008, **14**, 5073–5078.
47 A. Harada, R. Kobayashi, Y. Takashima, A. Hashidzume and H. Yamaguchi, *Nat. Chem.*, 2010, **3**, 34–37.
48 M. Nakahata, Y. Takashima, H. Yamaguchi and A. Harada, *Nat. Commun.*, 2011, **2**, 511.
49 S. Seiffert, *Angew. Chem., Int. Ed.*, 2013, **52**, 11462–11468.
50 Q. Wu, T. Su, Y. Mao and Q. Wang, *Chem. Commun.*, 2013, **49**, 11299–11301.
51 O. Kretschmann, S. W. Choi, M. Miyauchi, I. Tomatsu, A. Harada and H. Ritter, *Angew. Chem., Int. Ed.*, 2006, **45**, 4361–4365.
52 C. Koopmans and H. Ritter, *Macromolecules*, 2008, **41**, 7418–7422.
53 J. Liu, G. Chen, M. Guo and M. Jiang, *Macromolecules*, 2010, **43**, 8086–8093.
54 M. Ciampolini and N. Nardi, *Inorg. Chem.*, 1966, **5**, 41–44.
55 J. Wang and K. Matyjaszewski, *J. Am. Chem. Soc.*, 1995, **117**, 5614–5615.
56 K. Matyjaszewski and J. Xia, *Chem. Rev.*, 2001, **101**, 2921–2990.
57 D. G. Lessard, M. Ousalem and X. X. Zhu, *Can. J. Chem.*, 2001, **79**, 1870–1874.
58 Y. Xia, X. Yin, N. A. D. Burke and H. D. H. Stöver, *Macromolecules*, 2005, **38**, 5937–5943.
59 C. Alexander and K. M. Shakesheff, *Adv. Mater.*, 2006, **18**, 3321–3328.
60 T. Rossow, S. Bayer, R. Albrecht, C. C. Tzschucke and S. Seiffert, *Macromol. Rapid Commun.*, 2013, **34**, 1401–1407.
61 H. Ringsdorf, J. Venzmer and F. Winnik, *Macromolecules*, 1991, **24**, 1678–1686.
62 P. Wu, R. Q. Xiao, C. Q. Zhang, L. P. Zhou, Q. Luo, J. Y. Xu and J. Q. Liu, *Catal. Lett.*, 2010, **138**, 62–67.
63 X. Liao, G. Chen, X. Liu, W. Chen, F. Chen and M. Jiang, *Angew. Chem.*, 2010, **122**, 4511–4515.
64 T. M. Eggenhuisen, C. R. Becer, M. W. M. Fijten, R. Eckardt, R. Hoogenboom and U. S. Schubert, *Macromolecules*, 2008, **41**, 5132–5140.